Tight-binding molecular dynamics in liquid III-V compounds. II. Simulations for GaAs and GaSb

1994 J. Phys.: Condens. Matter 6 5255

(http://iopscience.iop.org/0953-8984/6/28/004)

J. Phys.: Condens. Matter 6 (1994) 5255–5271. Printed in the UK

Tight-binding molecular dynamics in liquid III–V compounds: II. Simulations for GaAs and GaSb

C Molteni, L Colombo and L Miglio
Dipartimento di Fisica dell'Università di Milano, via Celoria 16, I-20133 Milano, Italy

Received 5 April 1994

Abstract. We apply the tight-binding scheme developed in the preceding paper to molecular-dynamics simulations of liquid GaAs and GaSb. We investigate structural, electronic and dynamical properties of both liquid samples and present a comparison to experimental and *ab initio* data. Finally, we discuss the reliability of the present tight-binding method for molecular dynamics in III–V compounds.

1. Introduction

Tight-binding molecular-dynamics (TBMD) simulations have recently been demonstrated to be a reliable and accurate scheme in the case of elemental semiconductors, like silicon [1] in the crystalline, liquid and amorphous phases or carbon-based systems [2]. Since they allow the calculation of structural, electronic and dynamical properties for large supercells and long simulation times with a reduced computational workload, they are a suitable tool for material-science investigations of technologically interesting systems.

At variance with the simpler case of elemental materials, heterovalent compounds display polar bonds and non-negligible effects due to charge transfer. Besides, in liquid and amorphous samples, the presence of two atomic species allows the formation of different types of bond (between like and unlike atoms), giving rise to a more complex structural disorder where chemical defects like 'wrong bonds' (i.e. bonds between like atoms) are present. All these features make the extension of TBMD to III–V compounds not a trivial task.

In the preceding paper (hereafter referred to as part I), we have developed a simple interpolative method to reproduce the cohesion-energy phase diagram of GaAs, as obtained by *ab initio* calculations. We have derived a transferable tight-binding scheme to be used over a wide range of coordinations and geometries in molecular dynamics [3]. The critical choice of the repulsive part of the potential confirms the importance of charge-transfer effects in III–V compounds and supplies a physical insight into the different contributions to the interatomic potential.

We have selected two different parametrizations for GaAs, originated by two sets of *ab initio* input data (density-functional–LDA [4] (DFT–LDA) and Hartree–Fock plus correlation corrections [5] (HF+C)) and we have performed the simulation of the liquid phase of GaAs (l-GaAs), in order to compare their performances with existing experimental data [6] and theoretical [7, 8] predictions. We have also performed a simulation for l-GaSb, for which anion and cation sizes are remarkably different and our approaches (see part I) are more critical.

0953-8984/94/285255+17$19.50

With respect to a recent letter of ours [9], we report a larger amount of structural, dynamical and electronic information which demonstrates the reliability and transferability of our approach.

2. Computational framework

The total force acting on an atom has two contributions, deriving from the band-structure energy and from the repulsive potential (see (1), (2) of part I). More explicitly, the force acting on atom k in the x direction is expressed by the following relation:

$$F_{x_k}^{\mathrm{tot}} = F_{x_k}^{\mathrm{bs}} + F_{x_k}^{\mathrm{rep}} = -\frac{\mathrm{d}}{\mathrm{d}x_k}\left[2\sum_{n,k}^{\mathrm{occ}} \epsilon_n(k)\right] - \frac{\mathrm{d}}{\mathrm{d}x_k}\left[\sum_{i,j>i} U(r_{ij})\right]. \tag{1}$$

At variance with the ordered crystalline structures, first-neighbour bonds can now have different lengths r_{ij}, within a cut-off radius r_{cut}, whose value is generally halfway between first- and second-neighbour crystalline equilibrium distances. $F_{x_k}^{\mathrm{rep}}$ implies straightforward analytic derivatives, while $F_{x_k}^{\mathrm{bs}}$ is equal to the following expression (only the (001) point is used for the integration over the Brillouin zone):

$$F_{x_k}^{\mathrm{bs}} = -2\sum_{n}^{\mathrm{occ}} \sum_{i\alpha,j\beta} c_{i\alpha}^{(n)} c_{j\beta}^{(n)} \left[\frac{\partial}{\partial x_k} H_{i\alpha,j\beta}\right] \tag{2}$$

where $\{c_{i\alpha}^{(n)}\}$ are the expansion coefficients of the electronic wave function with respect to the atomic-like orbital basis and $H_{i\alpha,j\beta}$ are the TB matrix elements between the α-type orbital centred on site i ($\varphi_\alpha(r - r_i)$) and the β-type one centred on site j ($\varphi_\beta(r - r_j)$). We have used an sp^3s^* basis [12] as described in part I. By explicitly writing the previous equation

$$\begin{aligned} F_{x_k}^{\mathrm{bs}} = -2\sum_{n}^{\mathrm{occ}} \sum_{i\alpha,j\beta} c_{i\alpha}^{(n)} \langle \varphi_\alpha(r - r_i)| \frac{\partial}{\partial x_k} H |\varphi_\beta(r - r_j)\rangle c_{j\beta}^{(n)} \\ - 2\sum_{n}^{\mathrm{occ}} \sum_{i\alpha,j\beta} c_{i\alpha}^{(n)} \left[\left\langle \frac{\partial}{\partial x_k}\varphi_\alpha(r - r_i)|H|\varphi_\beta(r - r_j)\right\rangle \right. \\ \left. + \left\langle \varphi_\alpha(r - r_i)\,|H|\,\frac{\partial}{\partial x_k}\varphi_\beta(r - r_j)\right\rangle\right] c_{j\beta}^{(n)}. \end{aligned} \tag{3}$$

The first term represents the Hellmann–Feynman contribution [10], while the others are originated by the dependence of the basis function on the atomic coordinate x_k (Pulay's forces [11]).

The MD simulations have been performed with a cubic cell with periodic boundary conditions [13], containing 64 atoms. The integration algorithm for the equation of motion is the velocity Verlet one [14]. We have used a time step as large as $\sim 10^{-15}$ s, performing simulations in both the microcanonical and canonical ensembles. Heating and cooling of the samples are obtained by velocity rescaling. As previously mentioned, for the integration over the Brillouin zone, only the supercell (000) point has been used: this guarantees a

sufficiently accurate integration for a supercell containing 64 or more atoms. We have introduced a smooth interaction cut-off function [15], expressed by

$$f_{\rm cut}(r) = \frac{1}{2}\left[1 - \tanh\left(\frac{r - r_{\rm cut}}{\Delta}\right)\right] \tag{4}$$

where $r_{\rm cut}$ is the bond length and Δ is the scale on which the cut-off function decays. Since we work in the framework of a first-neighbour scheme, $r_{\rm cut}$ should have a value that lies in between the equilibrium first- and second-neighbour bond lengths, respectively r_0 and $1.63r_0$. We have chosen $r_{\rm cut} = 1.3r_0$ and $\Delta = 0.1$ Å.

In order to test our code, we have performed preliminary MD simulations with the $U(r) = \Phi_1 \exp[-(r - r_0)/\alpha] + \Phi_2(r_0/r)$ repulsive potential in the microcanonical ensemble for c-GaAs, in the ZnS geometry, at different temperatures (100, 300, 600 K); see figure 1. As expected, the system maintains the tetrahedral coordinations, with a broadening of the pair correlation function and the bond-angle distribution peaks, due to the temperature increase. The total energy is conserved within 10^{-5} eV atom^{-1}. No relevant differences are obtained if we use the DFT–LDA or the HF+C fitted potentials.

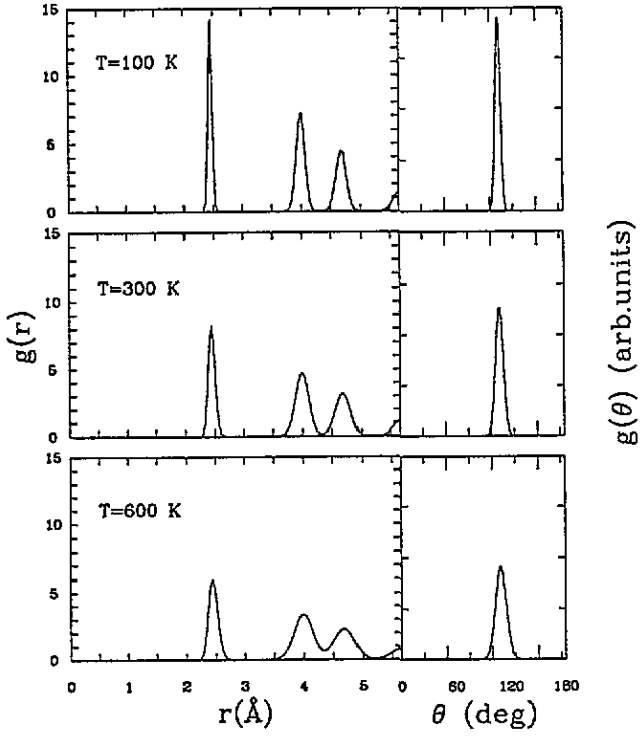

Figure 1. Pair correlation functions (left) and bond-angle distributions (right) for c-GaAs in the ZnS geometry at finite temperature (100, 300, 600 K).

3. TBMD simulation of liquid GaAs

3.1. Sample preparation

In order to melt GaAs, the atoms were initially arranged in a ZnS crystal structure, with a cell size reproducing the experimental liquid density at the melting point ($\rho = 5.71$ g cm^{-3}) [16]. Then, the temperature of the system was gradually raised to 3000 K, by rescaling ionic velocities during a $\sim$ 1.5 ps long annealing. After an equilibration of $\sim$ 1.5 ps, the temperature was gradually reduced (in $\sim$ 2 ps) to 1600 K, somewhat above the experimental melting point ($T_{\rm melt} = 1511$ K). The system was equilibrated at this temperature for 4 ps and, finally, observed for 5 ps. Apart for the time lengths of the various phases, this is exactly the same preparation method as used in [7] within a Car–Parrinello simulation. The results here reported have been obtained with the repulsive potential $U(r) = \Phi_1 \exp[-(r - r_0)/\alpha] + \Phi_2(r_0/r)$ where the parameters have been fitted to the DFT–LDA data (see part I). A critical comparison to the liquid simulation results obtained using the same repulsive potential fitted to the HF+C data and the method of the unconventional scaling function with parameters fitted to DFT–LDA data is reported in the last section.

3.2. Structural properties

Three pair correlation functions are required for a complete description of static two-body correlation functions in a binary compound [17]:

$$c_\beta \rho g_{\alpha\beta}(r) = \frac{1}{N_\alpha}\left\langle \sum_{i=1}^{N_\alpha}\sum_{j=1}^{N_\beta} \delta(r - (r_{\alpha i} - r_{\beta j}))\right\rangle - \delta_{\alpha\beta}\delta(r) \tag{5}$$

where $\alpha, \beta =$ Ga, As, $\rho = N/V$ is the number density ($\sim$ 0.04 atoms Å^{-3}), N_α is the number of type α atoms and $c_\alpha = N_\alpha/N$ the corresponding concentration. The $\langle \ldots \rangle$ brackets denote the ensemble average. The total pair correlation function is related to the partial ones by the relation

$$g(r) = c_{\rm Ga}^2 g_{\rm GaGa} + c_{\rm As}^2 g_{\rm AsAs} + 2c_{\rm Ga}c_{\rm As}g_{\rm GaAs}. \tag{6}$$

No experimental information is available for the partial correlation functions, while experimental data for the total pair correlation function are shown for comparison in figure 2: they have been obtained by Fourier transforming the corresponding structure factor as measured by neutron scattering [6]. The main features of $g(r)$ are well reproduced. In particular, the position and the intensity of the first peak (corresponding to the first-neighbouring cell) agree well with experiment, while the first minimum is slightly underestimated. By considering that the first-neighbour peak is the only relevant structure, we conclude that l-GaAs has a non-compact structure, nested shell by shell with an alternation of cation and anion shells. Further confirmation of this picture comes from the inspection of the $g_{\alpha\beta}$, which definitely differ from the ones typical of strongly ionic systems: the latter, in fact, display peaks and minima for like-atom correlations out of phase with respect to those for unlike atoms.

Two previous MD simulations in liquid GaAs are present in the literature: one based on pseudopotential-derived interatomic forces [8] and the other based on the Car–Parrinello method [7]. At variance with the former and in agreement with the latter, the atomic distribution found in the present simulation is not chemically random: a strong correlation

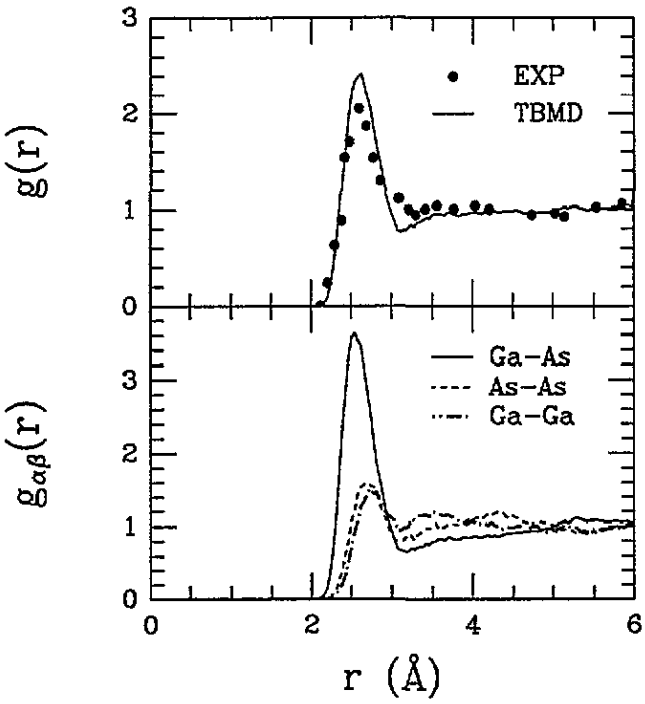

Figure 2. Total (top) and partial (bottom) pair correlation functions for l-GaAs at 1600 K. Experimental data from [6]

still occurs between anions and cations. The disagreement between the pseudopotential-derived interatomic-force simulation and both our TBMD and *ab initio* calculations is related to the spatial distribution of the two atomic species. This demonstrates that the use of a pair potential is successful only for a limited set of properties. For a complete description of l-GaAs an approach that includes in an explicit way, semiempirical or *ab initio*, the electronic structure is actually needed.

Partial structure factors [18] are defined by

$$S_{\alpha\beta} = \delta_{\alpha\beta} + 4\pi\rho(c_\alpha c_\beta)^{1/2}\int_0^\infty [g_{\alpha\beta}(r) - 1]\frac{\sin kr}{kr}r^2\,\mathrm{d}r. \tag{7}$$

It is convenient to build other structure factors as linear combinations of those defined above, to describe correlations between particle density and concentration fluctuations at a given wave vector [19]:

$$S_{NN}(k) = c_{\mathrm{Ga}}S_{\mathrm{GaGa}}(k) + c_{\mathrm{As}}S_{\mathrm{AsAs}}(k) + 2(c_{\mathrm{Ga}}c_{\mathrm{As}})^{1/2}S_{\mathrm{GaAs}}(k) \tag{8}$$

$$S_{cc}(k) = c_{\mathrm{Ga}}c_{\mathrm{As}}[c_{\mathrm{Ga}}S_{\mathrm{GaGa}}(k) + c_{\mathrm{As}}S_{\mathrm{AsAs}}(k) - 2(c_{\mathrm{Ga}}c_{\mathrm{As}})^{1/2}S_{\mathrm{GaAs}}(k)] \tag{9}$$

$$S_{Nc}(k) = c_{\mathrm{Ga}}c_{\mathrm{As}}\left[S_{\mathrm{GaGa}}(k) - S_{\mathrm{AsAs}}(k) + \frac{c_{\mathrm{As}} - c_{\mathrm{Ga}}}{(c_{\mathrm{Ga}}c_{\mathrm{As}})^{1/2}}S_{\mathrm{GaAs}}(k)\right]. \tag{10}$$

The neutron-scattering intensity itself is a linear combination of the partial structure factors $S_{\alpha\beta}$, with weighting factors given by products of the scattering amplitudes of the component

species:

$$S(k) = \frac{\left[b_{\mathrm{Ga}}^2 S_{\mathrm{GaGa}}(k) + b_{\mathrm{As}}^2 S_{\mathrm{AsAs}}(k) + 2b_{\mathrm{Ga}} b_{\mathrm{As}} S_{\mathrm{GaAs}}(k)\right]}{b_{\mathrm{Ga}}^2 + b_{\mathrm{As}}^2} \tag{11}$$

where $b_{\mathrm{Ga}} = 7.2$ fm and $b_{\mathrm{As}} = 6.7$ fm are the experimental neutron-scattering lengths [20]. The $S(k)$ obtained in this way is practically indistinguishable from $S_{NN}(k)$. In figures 3 and 4 we show the TBMD structure factor for liquid GaAs together with neutron-scattering data and the number-concentration structure factors, respectively.

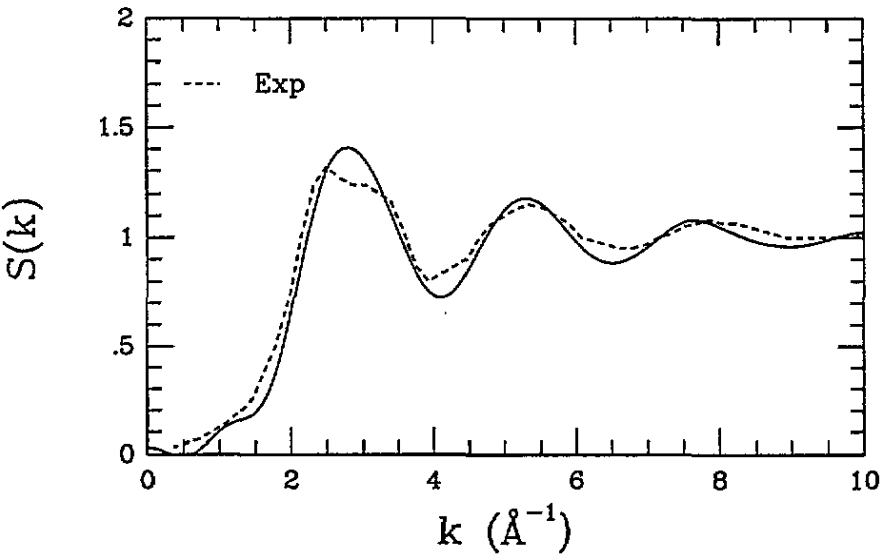

Figure 3. Structure factor for l-GaAs: TBMD calculation (solid line) and experimental [6] neutron-scattering results (dashed line).

The main features are pretty well reproduced with the exception of the shoulder in the experimental first peak. This is, however, an important feature (missed both by *ab initio* and semiempirical simulations) that indicates how the covalent character of l-GaAs is somewhat underestimated.

The first-neighbour shell is delimited by the first minimum of $g(r)$, that in this particular case coincides with the cut-off radius r_{cut}). Accordingly the average coordination number of l-GaAs was calculated to be 5.997, to be compared with the experimental value of (5.5 ± 0.5): each Ga has on average 5.968 neighbours (2.06 Ga and 3.908 As), while As atoms have 6.025 neighbours (2.117 Ga and 3.908 As). All this information and a more detailed coordination distribution are summarized in figure 5. The coordination number is quite low if compared to that of simple liquid metals (12–14) and even lower than that of l-Si and l-Ge (six to seven) [21]: this is due to the preferential bonds between unlike atoms that persist even in the liquid phase. In fact, even if the average coordination is almost six, the effective Ga–As coordination remains tetrahedral. The value of the average coordination number calculated by first principles is 6.3: each Ga/As has 2.6/2.2 first neighbours of the same and 3.9 of the other species. These numbers are obviously dependent on the definition of the maximum first-neighbour distance, which is dictated by the $g(r)$ behaviour.

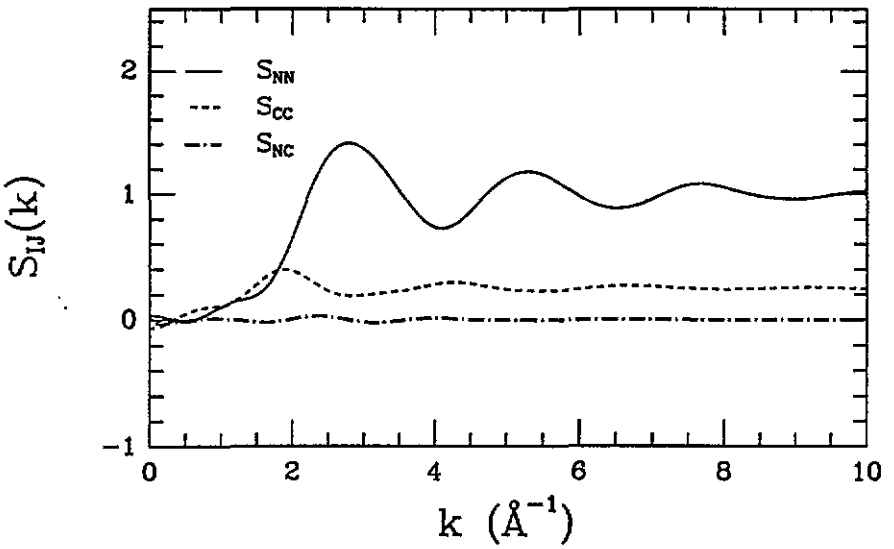

Figure 4. Number–concentration structure factors S_{IJ} $(I, J = N, c)$ for l-GaAs: S_{NN} (solid line); S_{cc} (dashed line); S_{Nc} (dashed–dotted line).

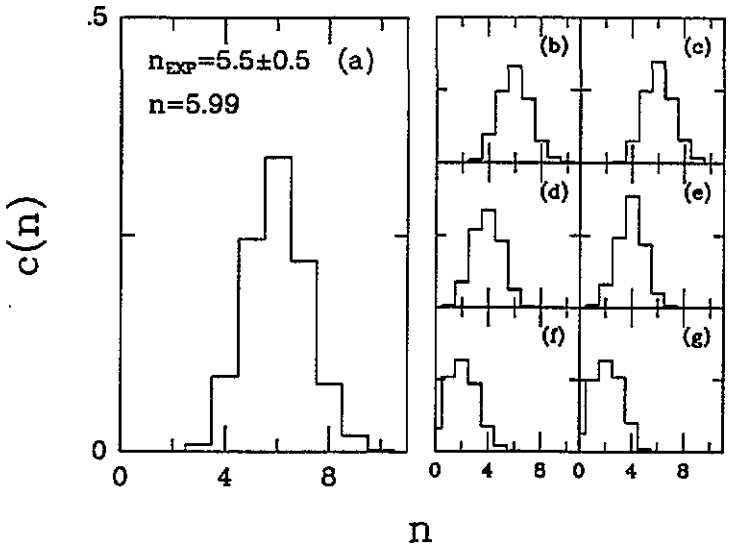

Figure 5. Total (a) and partial coordination functions: (b) Ga–X (probability for a Ga atom to have n first neighbours of type X=Ga,As); (c) As–X; (d) Ga–As; (e) As–Ga; (f) Ga–Ga; (g) As–As.

Important information about the short-range arrangement comes from the bond-angle distributions:

$$g(\theta) = \left\langle \sum_{i=1}^{N} \sum_{j=1}^{N} \sum_{j'(\neq j)=1}^{N} \delta(\theta - \theta_{jj'}^{i}) \right\rangle \tag{12}$$

where j and j' label two first neighbours of the atom i and $\theta_{jj'}^{i}$ is the bond angle, with the

vertex at i, between j and j'. The total bond-angle distribution, displayed in figure 6(a), shows two main structures: one around 104° (reminiscent of the tetrahedral bonding) and the other around 60° (typical of compact coordinations, such as the FCC one). By considering that the cationic and anionic sublattices are FCC in crystalline GaAs, we can argue that the 60° peak is mainly determined by atoms in second-neighbour positions that are close enough to the pivot atom to fall within the cut-off radius. This feature is similarly found in silicon [21] and turns out to be a general property of covalent liquids. In figure 6 several partial bond-angle distributions confirming our analysis are displayed. The partial bond-angle distributions concern the following cases: X–Ga–X (where the central atom is the pivot and X = Ga, As) (b); X–As–X (c); As–Ga–As (d); Ga–As–Ga (e); Ga–Ga–Ga (f) and As–As–As (g). We observe that the 60° peak intensity in panels (d) and (e) decreases to indicate that it represents contributions from angles made by pairs of unlike atoms centred around a Ga or an As. The occurrence of Ga–Ga–Ga and As–As–As triplets is rather infrequent. The shape of bond-angle distribution functions, as well as the coordination functions, critically depends on the definition of the maximum first-neighbour distance. If this quantity is reduced in the bond-angle distribution calculation, the 60° peak vanishes and the tetrahedral structure dominates.

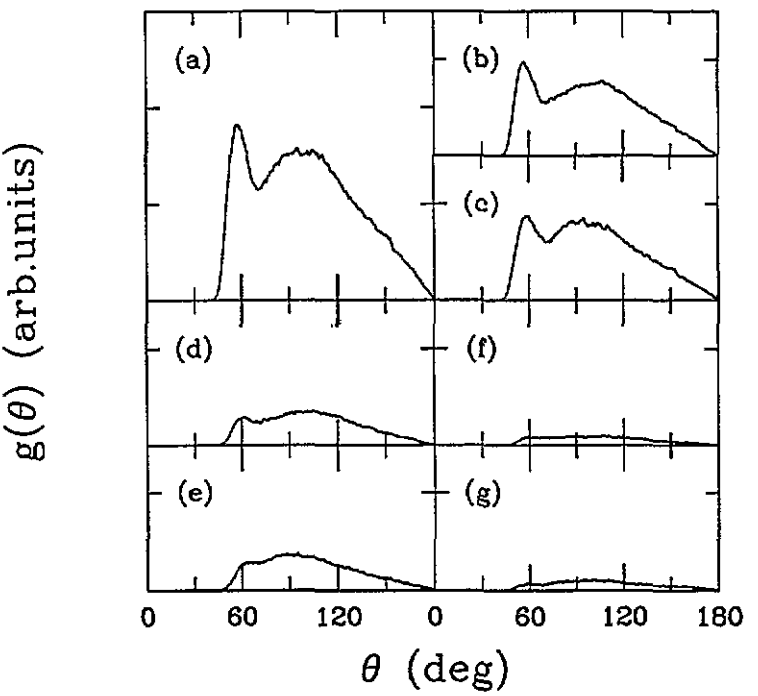

Figure 6. Total and partial bond-angle distributions for l-GaAs: (a) total; (b) X–Ga–X; (c) X–As–X; (d) As–Ga–As; (e) Ga–As–Ga; (f) Ga–Ga–Ga; (g) As–As–As.

3.3. Dynamical properties

The diffusive behaviour of the l-GaAs sample is demonstrated by the linear behaviour of the mean-square displacement:

$$\langle r^2(t)\rangle = \frac{1}{N}\sum_{i=1}^{N}[r_i(t) - r_0(t)]^2. \tag{13}$$

The velocity autocorrelation function is defined as follows:

$$Z(t) = \frac{\sum_{i=1}^{N} v_i(t)\cdot v_i(t_0)}{\sum_{i=1}^{N} v_i(t_0)\cdot v_i(t_0)} \tag{14}$$

where t_0 is the time origin of the observation and v_i are the atomic velocities. By restricting the summation only to atoms of the same kind, the cationic and anionic velocity–velocity autocorrelation functions are obtained. Finally, by integrating them, the self-diffusion coefficients are calculated as

$$D_\alpha = \frac{k_B T}{M_\alpha}\int_{t_0}^{\infty} Z_\alpha(t)\,dt \tag{15}$$

where α, β = Ga, As, k_B is Boltzmann's constant, T the temperature and M_α the cationic or anionic mass. The self-diffusion coefficient values for l-GaAs are $D_{Ga} = 1.006 \times 10^{-4}$ cm^2 s^{-1} and $D_{As} = 0.722 \times 10^{-4}$ cm^2 s^{-1}, with an average value $D = 0.864 \times 10^{-4}$ cm^2 s^{-1} to be compared with an experimental datum [22] of 1.6×10^{-4} cm^2 s^{-1} and with the *ab initio* [7] results: $D_{Ga} = 1.6 \times 10^{-4}$ cm^2 s^{-1} and $D_{As} = 1.2 \times 10^{-4}$ cm^2 s^{-1}.

The systematically lower values of the TBMD diffusion coefficients with respect to experimental and *ab initio* results seem to suggest that the TB potential favours in a sense the tetrahedral coordination. It is, thus, likely that, using the same potential with parameters fitted to the HF+C data, lower diffusion coefficients will be obtained. The vibrational density of states is obtained by Fourier transforming $Z(t)$ and it is plotted in figure 7, together with the corresponding autocorrelation function. The system shows clearly a liquid behaviour, with modes at zero frequency. Still, a shoulder around 7 THz keeps track of the crystalline optical modes. In l-GaAs, the oscillations of the velocity–velocity autocorrelation function rapidly vanish after a short time, as expected. The correlation time, representing the time needed for the system to lose its memory of the initial conditions, is 0.4 ps.

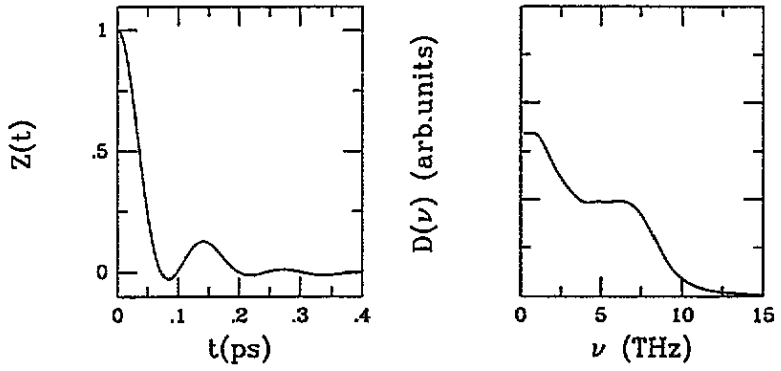

Figure 7. Velocity autocorrelation function (left) and vibrational density of states (right) for l-GaAs.

Among all the calculated properties, the main differences with respect to *ab initio* results appear in the vibrational density of states. They are in fact extremely sensitive to details in the potentials that influence the structural and electronic properties only in a negligible way. It is likely that a more refined fit of the potential parameters, including information from the bulk moduli, can reproduce the vibrational properties more accurately.

3.4. Electronic properties

In the ZnS crystalline phase with tetrahedral coordination, c-GaAs is a semiconducting material, while in the higher-coordination geometries, NaCl and CsCl, it shows a metallic behaviour. In the liquid phase, GaAs is found to be a metal, like l-Si [21]. In figure 8 we show the electronic density of states (top panel) and its cationic (middle panel) and anionic (bottom panel) contributions projected on s, p and s* states. Some features of the ZnS crystalline density of states persist in the liquid, like the s As band at low energies. The metallic behaviour, typical also of the crystalline NaCl and CsCl geometries, can be attributed to the augmented coordination with respect to the tetrahedral case.

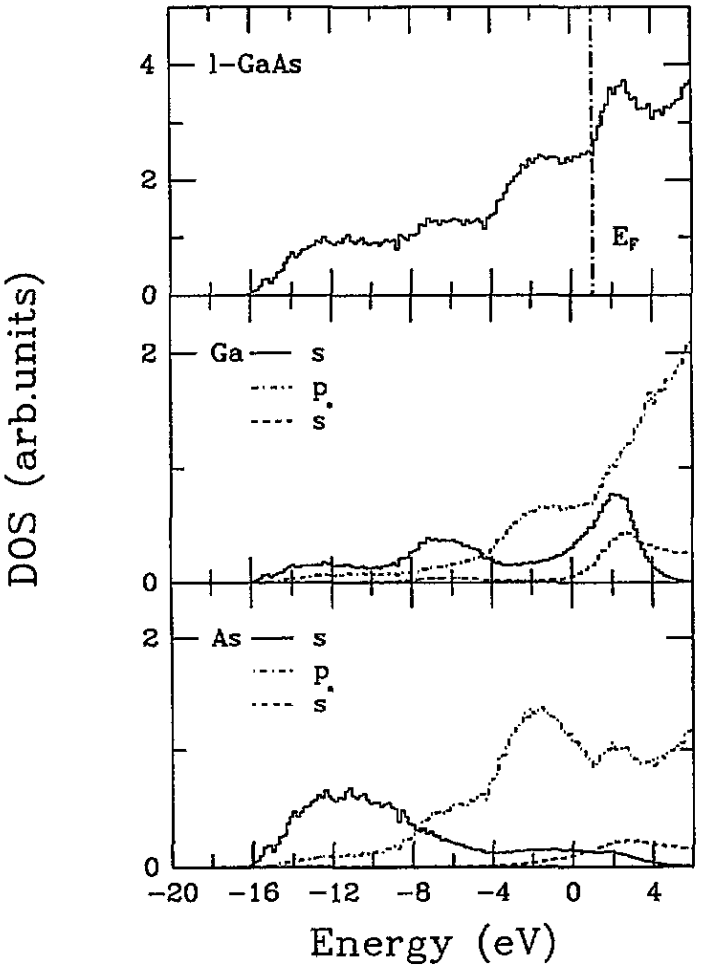

Figure 8. Electronic density of states (top) and its cationic (middle) and anionic (bottom) contributions, projected on s, p and s* states for l-GaAs. The dashed–dotted line in the top panel indicates the Fermi level.

Contributions from s* states are limited mainly to conduction states, as expected: the use of the excited s* state is the simplest way to reproduce well not only the valence bands, but also the lowest conduction band, maintaining a first-neighbouring approach.

4. Simulation for liquid GaSb

The liquid structure of GaSb has been recently studied by means of neutron diffraction [23]. The TBMD method has been applied also to this compound, characterized by a remarkable difference in the anion and cation sizes. In this way, we can verify the validity of the assumptions made for the repulsive like-atom interactions in a case other than GaAs.

We use a periodically repeated cubic cell, containing 64 atoms, and a time step of $\sim 1.5 \times 10^{-15}$ s. The repulsive potential is $U(r) = \Phi_1 \exp[-(r - r_0)/\alpha] + \Phi_2(r_0/r)$, with parameters fitted to DFT–LDA data [24] (see part I). A ZnS crystalline sample has been heated up to 2000 K in 2.25 ps, then, after 2.25 ps of equilibration, cooled in 3 ps down to 1350 K. Statistics were collected (after a further equilibration of 3 ps) for 7.5 ps. Other observations have been performed at 1200 and 1100 K.

The behaviour is qualitatively similar to that of l-GaAs, even if, in the partial $g_{\alpha\beta}(r)$, the cation–cation correlations are quite different from the anion–anion ones. In fact, as shown in figure 9, the Ga atoms tend to coordinate each other at greater distances than the Sb ones.

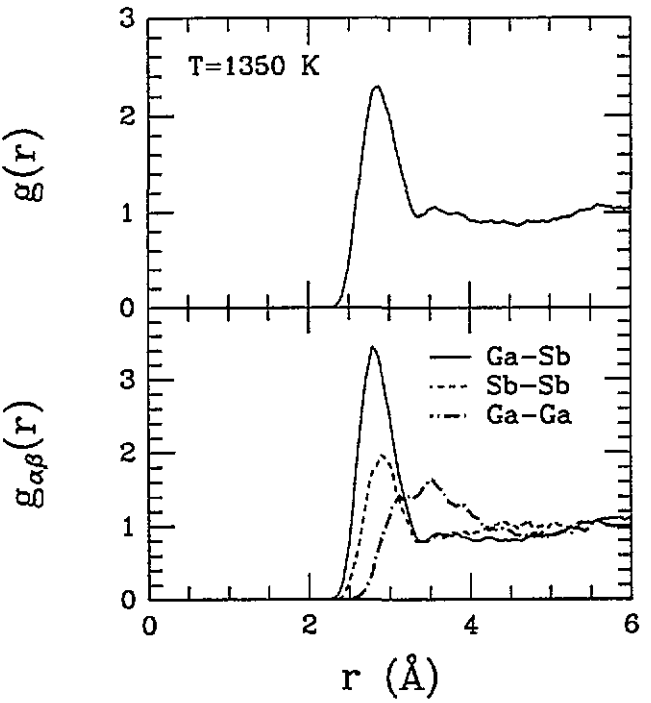

Figure 9. Total (top) and partial (bottom) pair correlation functions for l-GaSb at 1350 K.

Within a 3.434 Å radius, at 1350 K, the average coordination number is 6.07, to be compared with an experimental evaluation of (5.4±0.5). The structure factor is qualitatively well reproduced even if, as in the case of l-GaAs, we fail to reproduce the experimental shoulder of the first peak (see figure 10). The bond-angle distributions (shown in figure 11) are similar to the ones calculated for l-GaAs with a minor peak around 60° and a broad main structure around 100°. At variance with the previously studied case the maximum of $g_{\mathrm{Ga-Sb-Ga}}(\theta)$ is around 80°.

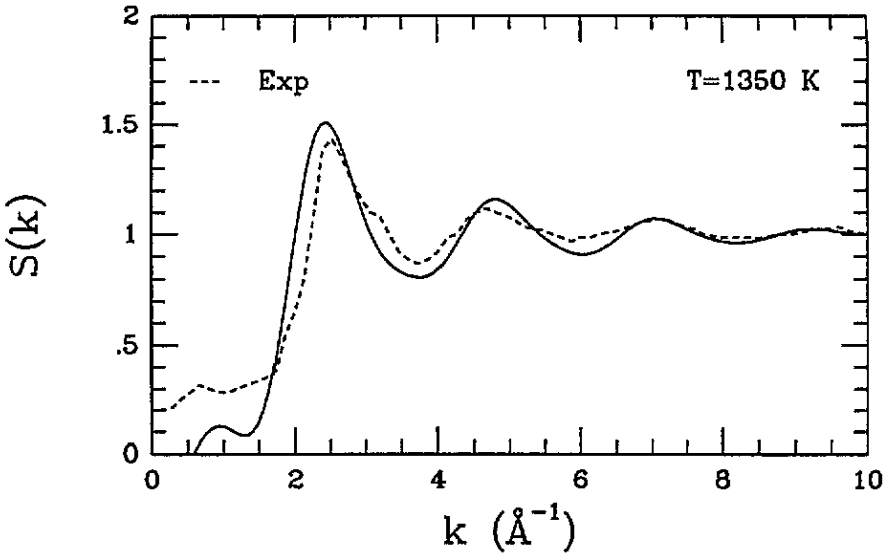

Figure 10. Structure factor for l-GaSb at 1350 K: TBMD calculation (solid line) and experimental [23] neutron-scattering results (dashed line).

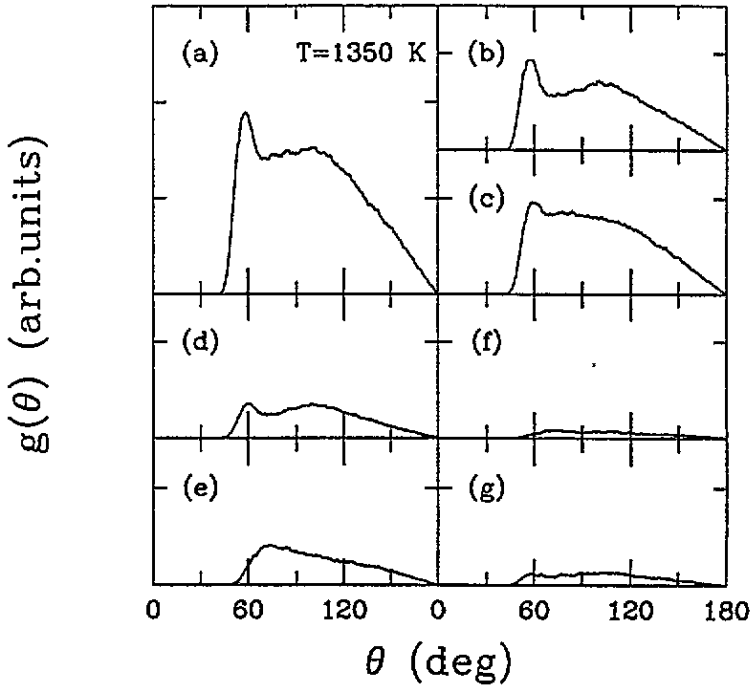

Figure 11. Total and partial bond-angle distributions for l-GaSb at 1350 K: (a) total; (b) X–Ga–X; (c) X–As–X; (d) As–Ga–As; (e) Ga–As–Ga; (f) Ga–Ga–Ga; (g) As–As–As.

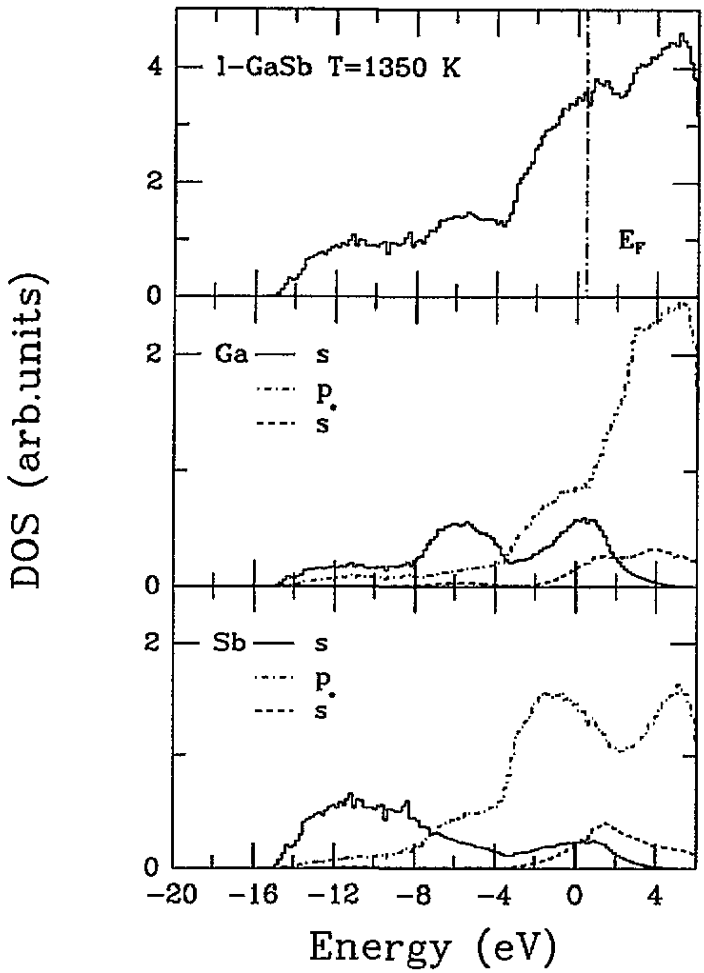

Figure 12. Electronic density of states (top) and its cationic (middle) and anionic (bottom) contributions, projected on s, p and s* states for l-GaSb at 1350 K. The dashed–dotted line in the top panel indicates the Fermi level.

As for the electronic structure, l-GaSb was found to be a metal, like l-GaAs. The density of states is shown in figure 12.

The self-diffusion coefficients, calculated through equation (15), are reported in table 1 for three different temperatures. The calculated vibrational densities of states are typical of liquid samples, displaying zero-frequency modes. The number of $\nu = 0$ diffusive modes decreases with the temperature decrease.

Table 1. Diffusion coefficients for l-GaSb at three different temperatures.

	1350 K	1200 K	1100 K
D_{Ga} (10^{-4} cm^2 s^{-1})	0.95	0.84	0.72
D_{Sb} (10^{-4} cm^2 s^{-1})	0.71	0.54	0.47
D (10^{-4} cm^2 s^{-1})	0.83	0.69	0.60

The criteria for selecting the repulsive potential parameters still deserve a final comment. By using the same parameters for cation–anion, anion–anion and cation–cation pairs, the available experimental information has been qualitatively reproduced. The different behaviour of cations and anions has suggested to us to test whether different repulsive potentials for like atoms give better results. Having no data for the fitting, we have tried to use the same functional form of the repulsive potential, substituting $r_0 = r_{Ga-As}$ (2.64 Å) with the suitable characteristic distances r_{Ga-Ga} (2.46 Å) and r_{Sb-Sb} (2.65 Å) [25]. The potential has thus the form

$$U(r) = \Phi_1 \exp[-(r - r_{xy})/\alpha] + \Phi_2(r_{xy}/r) \tag{16}$$

where xy stands for Ga–Sb, Ga–Ga or Sb–Sb. In this case the repulsive potential for a Ga–Ga pair is less intense with respect to the previous case, so that cations can approach each other more easily.

Following the same thermal cycle as above, we obtained the pair correlation functions of figure 13, where a too strong correlation between like atoms and a consequent weakening of the unlike-atom interactions occur. The average coordination number is now 6.0, but each Ga has 6.51 neighbours (4.14 Ga and only 2.37 Sb) and each Sb has 5.48 neighbours (3.11 Sb and 2.37 Ga). The comparison to the experimental neutron-scattering results is worse than in the previous case, so that the best potential is the one which prevents bonds between like atoms. Probably this is a feature which should be ascribed to the band-structure part (here not self-consistent) rather than to the repulsive term.

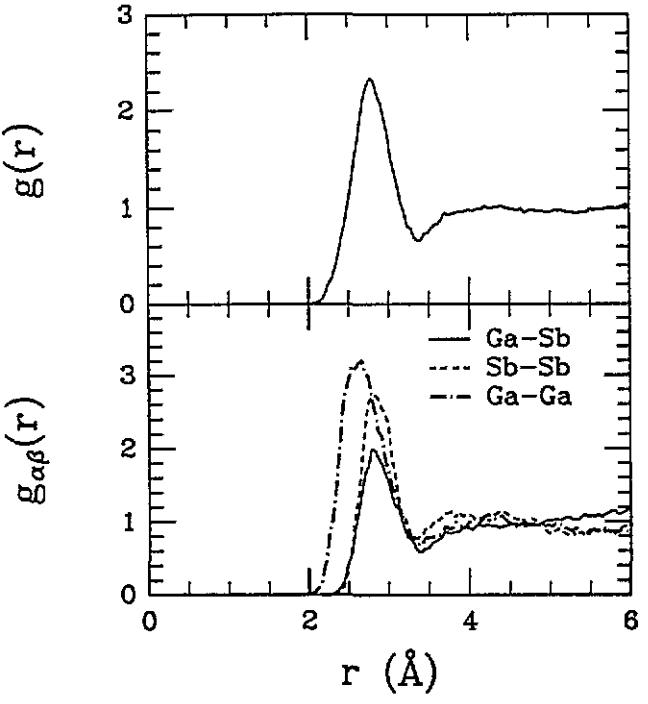

Figure 13. Total (top) and partial (bottom) pair correlation functions for l-GaSb at 1350 K: calculations using distinct repulsive Ga–Sb, Ga–Ga and Sb–Sb interactions (see text).

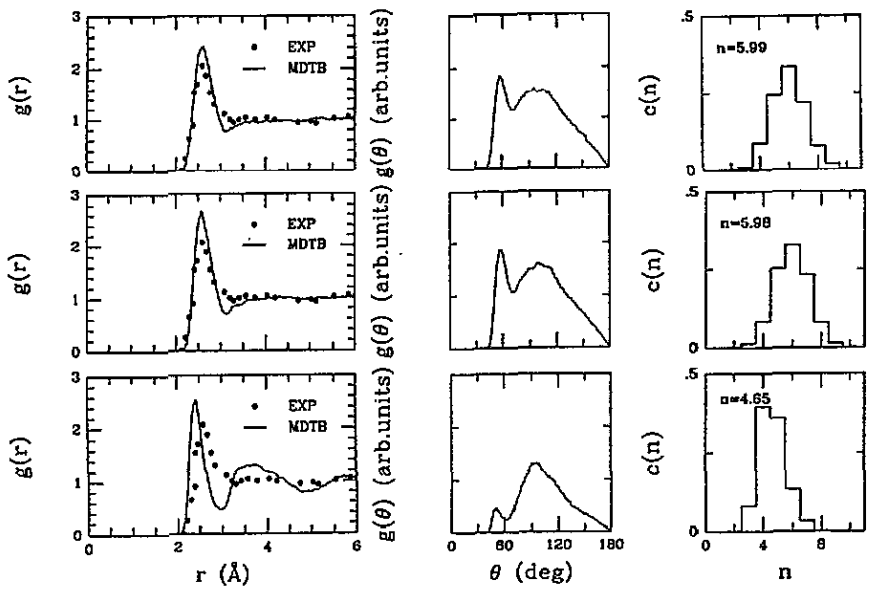

Figure 14. Pair correlation functions (left), bond-angle distributions (middle) and coordination functions (right) for l-GaAs at 1600 K, calculated using the $U(r) = \Phi_1 \exp[-(r - r_0)/\alpha] + \Phi_2(r_0/r)$ repulsive potential fitted to DFT–LDA (top) and HF+C (middle) data and with the unconventional scaling function method (bottom) fitted to DFT–LDA.

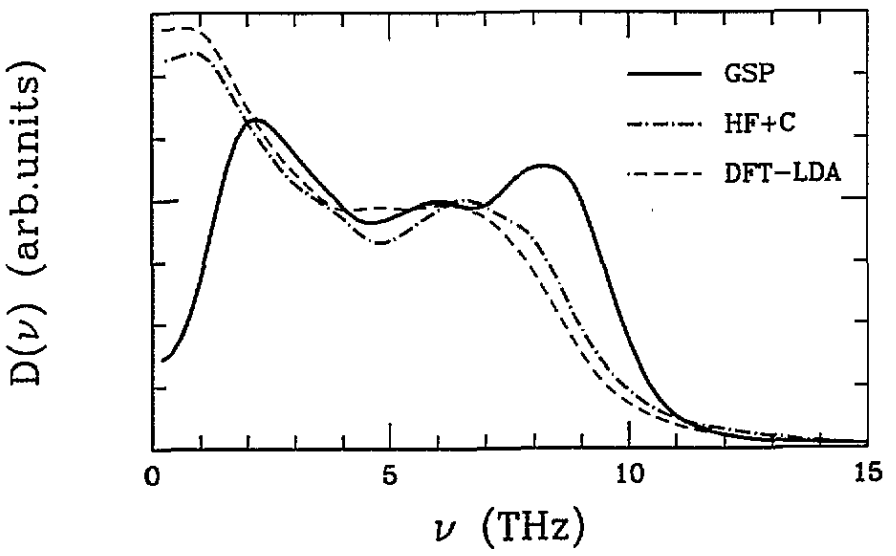

Figure 15. Vibrational density of states for l-GaAs at 1600 K, calculated using the $U(r) = \Phi_1 \exp[-(r - r_0)/\alpha] + \Phi_2(r_0/r)$ repulsive potential fitted to DFT–LDA (dashed line) and HF+C (dashed–dotted line) data and with the unconventional scaling function method (solid line) fitted to DFT–LDA.

5. Comparison among different potentials for liquid GaAs

The same simulation, presented for l-GaAs in section 3, has been performed also with $U(r) = \Phi_1 \exp[(r - r_0)/\alpha] + \Phi_2(r_0/r)$ fitted to the HF+C data and with the potential derived from the unconventional scaling function method, fitted to the DFT–LDA results (see part I).

The HF+C liquid turns out to be slightly more structured, but qualitatively it presents the same structural features as the DFT–LDA one. The main differences appear in the dynamical properties, as one can expect also from the comparison of the total-energy curves. The self-diffusion coefficients turn out slightly lower ($D_{Ga} = 0.734 \times 10^{-4}$ cm^2 s^{-1}; $D_{As} = 0.714 \times 10^{-4}$ cm^2 s^{-1} and $D = 0.724 \times 10^{-4}$ cm^2 s^{-1}) and the vibrational density of states shows a more pronunced shoulder around 7 THz. Therefore the liquid is more 'ordered' and stiff. However no remarkable differences are observed in the bond-angle distribution functions or the electronic density of states.

Large differences appear in the case of the simulations with the potential using unconventional scaling. In order to reach a diffusive behaviour, the system has now to be heated up to 5000 K instead of 3000 K. However the final results are definitely far from the experimental data and from the previously obtained results. Essentially, the sample remains extremely structured and, in spite of the high temperature reached in the preparation thermal cycle, a small number of like-atom bonds has formed. The average coordination number is 4.65: each Ga has 4.70 (0.82 Ga and 3.88 As) and each As has 4.59 (0.71 As and 3.88 Ga) neighbours. In particular a serious difficulty in the 'wrong-bond' formation is observed. The total bond-angle distribution displays the tetrahedral peak broadened by the increased disorder and a really low-intensity 60° structure. The solid-like behaviour of this sample is shown also by the electronic density of states: the semiconducting gap of c-GaAs is only partially filled in this case. The vibrational density of states does not show zero-frequency modes, typical of liquid samples, and the self-diffusion coefficients are $D_{Ga} = 0.097 \times 10^{-4}$ cm^2 s^{-1}; $D_{As} = 0.049 \times 10^{-4}$ cm^2 s^{-1} and $D = 0.073 \times 10^{-4}$ cm^2 s^{-1}, an order of magnitude lower than the ones previously calculated and the experimental data.

Comparisons among the pair correlation functions, the coordination functions, the total bond-angle distribution functions and the vibrational density of states as calculated by the three methods are reported in figures 14 and 15.

The potential with the unconventional scaling function has been demonstrated to be not fully adequate for molecular-dynamics applications. From the analysis of the three sets of results, we deduce that in order to perform MD simulations, it is essential to obtain the correct functional form for the potential, whereas the numerical values of the parameters (i.e. the *ab initio* set used for the fitting procedure), in the framework of the correct potential, are less important.

As a final comment we stress that our model is particularly useful since no electronic degrees of freedom are explicitly introduced in the molecular dynamics, so that large time steps are possible and, in turn, large simulation times. Moreover, by introducing the $1/r$ term, we also avoid self-consistent iterations and a site dependence, as in the embedded-atom model, is straightforwardly introduced.

Acknowledgments

We thank M Causà (University of Torino) and S de Gironcoli (SISSA, Trieste) for total-energy *ab initio* calculations, G Pacchioni (University of Milano) and J Skofronic

and the Supercomputer Calculation Research Institute of the Florida State University for computational support and G Benedek (University of Milano) for helpful discussions.

References

[1] Wang C Z, Chan C T and Ho K M 1991 *Phys. Rev. Lett.* **66** 189
Virkkunen R, Laasonen K and Nieminen R M 1991 *J. Phys.: Condens. Matter* **3** 7455
Servalli G and Colombo L 1993 *Europhys. Lett.* **22** 107
[2] Wang C Z, Ho K M and Chan C T 1993 *Phys. Rev. Lett.* **70** 611
Zhang B L, Wang C Z and Ho K M 1992 *Chem. Phys. Lett.* **193** 225
Zhang B L, Wang C Z, Ho K M, Xu C H and Chan C T 1992 *J. Chem. Phys.* **97** 5007
[3] Molteni C, Miglio L and Colombo L 1992 *Il Vuoto* **4** 94
[4] Froyen S and Cohen M 1983 *Phys. Rev.* B **28** 3258
[5] M Causà 1992 private communication
[6] Bergman C, Bichara C, Chieux P and Gaspard J P 1985 *J. Physique. Coll.* **46** C8 97
[7] Zhang Q M, Chiarotti G, Selloni A, Car R and Parrinello M 1990 *Phys. Rev.* B **42** 5071
[8] Hafner J and Jank W 1989 *J. Phys.: Condens. Matter* **1** 4325
[9] Molteni C, Colombo L and Miglio L 1993 *Europhys. Lett.* **24** 659
[10] Feynman R P 1939 *Phys. Rev.* **56** 340
[11] Pulay P 1969 *Mol. Phys.* **17** 197
[12] Vogl P, Hjalmarson H P and Dow J P 1983 *J. Phys. Chem. Solids* **44** 365
[13] Allen M P and Tildesley D J 1986 *Computer Simulations of Liquids* (Oxford: Oxford Science)
[14] Swope W C, Andersen H, Barens P H and Wilson K R 1982 *J. Chem. Phys.* **76** 637
[15] Khan F S and Broughton J Q 1989 *Phys. Rev.* B **39** 3688
[16] Glazov V M, Chizhevskaya S N and Glagoleva N N 1969 *Liquid Semiconductors* (New York: Plenum)
[17] Ashcroft N W and Langreth D C 1967 *Phys. Rev.* **156** 685
[18] March N H and Tosi M P 1991 *Atomic Dynamics in Liquids* (New York: Dover)
[19] Bathia A B and Thornton D E 1970 *Phys. Rev.* B **2** 3004
[20] Koester L 1977 *Neutron Physics (Springer Tracts in Modern Physics 90)* ed G Hohler (Berlin: Springer)
[21] Stich I, Car R and Parrinello M 1991 *Phys. Rev.* B **44** 4262
[22] Hellwege K H (ed) 1984 *Landölt–Bornstein New Series* (Berlin: Springer) p 3412
[23] Mizuki J, Kamimoto K, Misawa M and Fukuaga T 1993 *J. Phys.: Condens. Matter* **5** 3391
[24] de Gironcoli S 1993 private communication
[25] O'Reilly E P and Robertson J 1986 *Phys. Rev.* B **34** 8684